Japanese Journal of Applied Physics **49** (2010) 07HF08 **REGULAR PAPER**

Aberration Correction with Low-Frequency Transmission for Medical Acoustic Imaging

Hirofumi Taki* and Toru Sato

Graduate School of Informatics, Kyoto University, Yoshida-honmachi, Sakyo-ku, Kyoto 606-8501, Japan

Received November 24, 2009; accepted February 24, 2010; published online July 20, 2010

Phase aberration is one of the major causes of deterioration in the quality of medical acoustic imaging. To suppress the effect of aberration, we employ a focused transmit beam with a low center frequency for the calculation of an aberration correction value set. The aberration correction value set is applied to an imaging process utilizing high-frequency transmission. To evaluate the focus quality under severe aberration conditions, we introduce an evaluation criterion for beam patterns using the second moment of the acoustic field. The result implies that in severe aberration conditions without aberration correction, a low-frequency transmission acquires a better beam pattern, and the aberration correction value set for a high-frequency transmission should be calculated using a low-frequency transmission.

DOI: 10.1143/JJAP.49.07HF08

1. Introduction

One of the major causes of deterioration in medical acoustic imaging quality is phase aberration occurring from the distortion of the medium, where the main source of aberration is the human body wall. Many acoustic imaging methods for the improvement of spatial resolution introduce assumptions without aberration, and thus the efficiency of the methods has not been verified under severe aberration conditions.[1–4] Since the 1990s, many researchers have investigated harmonic imaging for medical application. In this method, the center frequency for a transmit event is different from that of a receive event.[5,6] Harmonic imaging has higher contrast resolution than fundamental imaging, and thus has become a standard choice of image modality in a clinical setting.[7,8] However, Varslot and coworkers showed that the aberration of the second harmonic is strongly related to the aberration of the first harmonic, and so harmonic imaging does not solve the problem of aberration.[9,10]

Flax and O'Donnell proposed an aberration correction method using estimated arrival time differences between adjacent elements.[11,12] Måsøy *et al.* compared two aberration correction methods for the estimation of time delay and amplitude fluctuations.[13] Many researchers have investigated transmit-beam aberration correction;[14–17] however, technological challenges still remain.

A large proportion of aberration correction methods utilize an iteration process. An initial value set of aberration correction values should be close to a true value set for the aberration values to converge and to decrease the number of iterations. In this study, we evaluate the accuracy of the time delay estimation from the cross-correlation coefficient utilizing acoustic pulses of low transmit frequency with no iteration process.

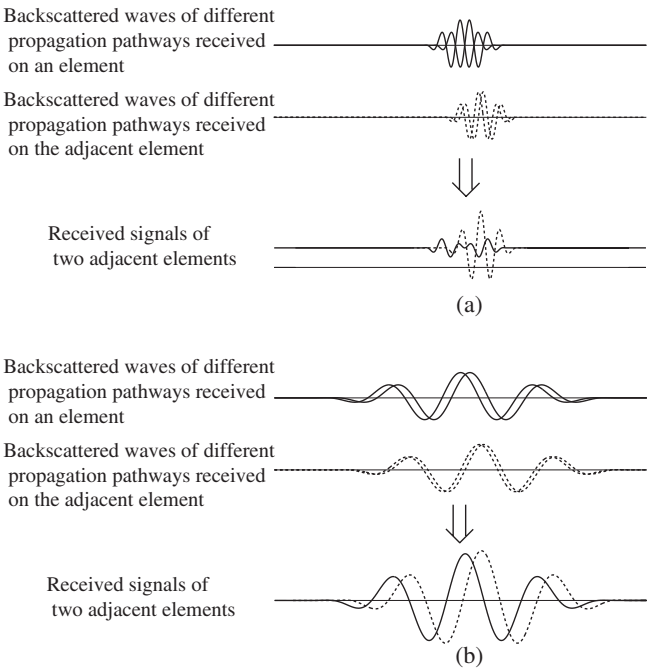

Fig. 1. Schema of decorrelation between the received signals at two adjacent array elements caused by aberration. A signal received at an element consists of several backscattered waves through different pathways in the Fresnel zone. (a) When a high-frequency transmit pulse is employed, the difference in path length caused by aberration changes the waveform of the received signal markedly from that of a backscattered wave. This causes the decorrelation between the received signals at two adjacent elements and the failure of estimation of arrival time difference between adjacent elements. (b) When a low-frequency transmit pulse is employed, the difference in path length slightly affects the waveform of the received signal. Therefore, the arrival time difference between adjacent elements is estimated successfully.

2. Methods

2.1 Aberration correction with low-frequency transmission

Aberration is caused by inhomogeneity of sound velocity in a propagation medium. Backscattered waves arrive at an element through the Fresnel zone, and thus the signal received at an element consists of several backscattered waves through different pathways. Since the inhomogeneity of sound velocity corresponds to the difference in the path length from that in an ideal homogeneous medium, the phase difference becomes larger when using higher frequency transmission. As shown in Fig. 1, when a high-frequency transmit pulse is employed, the difference in path length caused by aberration changes the waveform of the received signal markedly from that of a backscattered wave. This causes the decorrelation between the received signals at two adjacent elements and the failure of estimation of arrival time difference between adjacent elements. On the other hand, when a low-frequency transmit pulse is employed, the difference in path length slightly affects the waveform of the received signal. Therefore, arrival time difference between adjacent elements is estimated successfully. We therefore

*E-mail address: hirofumi.taki@mb6.seikyou.ne.jp

employed a focused transmit pulse of a low center frequency to increase the similarity of the received signals at two adjacent array elements for the accurate estimation of the aberration values. The aberration values estimated from the low transmit frequency were applied to the high transmit frequency event in acquiring the acoustic image with high spatial resolution. The cross-correlation value was

$$R(x,\tau) = \frac{\int_{z_1}^{z_2} g(x,z)g(x+\Delta X, z+c\tau)\,dz}{\sqrt{\int_{z_1}^{z_2} |g(x,z)|^2\,dz \int_{z_1}^{z_2} |g(x+\Delta X, z+c\tau)|^2\,dz}}, \quad (1)$$

where x and z are the lateral and vertical components of a measurement point P on a B-mode image, $g(x,z)$ is the acoustic RF signal at $P(x,z)$, ΔX is the element interval, and Z_1 and Z_2 are the minimum and maximum of the z coordinates in a region of interest (ROI) around the focus, respectively. The time delay value for the aberration correction, τ_x, is equal to τ when $R(x,\tau)$ is maximized under a condition of constant x. We set τ_x, the time delay value between adjacent array elements, to less than one half of a wavelength to remove the selection among false correlation peaks.

2.2 Equivalent half power width

To evaluate the focus quality of the proposed aberration correction methods, many researchers have utilized transmit beam patterns. In the presence of severe aberration, a transmit beam pattern deteriorates significantly. Therefore, investigating only the main lobe width and the sidelobe level of a transmit beam is not sufficient for an evaluation of the focus quality. Mallart and Fink.[17] proposed a focusing criterion based on the van Cittert–Zernike theorem; however, this criterion assumes that the medium is homogeneous.

To evaluate the focus quality of a transmit beam, it is necessary to investigate the following factors: main lobe width, peak intensity of main lobe, main lobe jitter, peak intensity of sidelobe, and the power summation of sidelobes. In addition, a single evaluation value for the focus quality is required to grade the proper transmit frequency for aberration correction. Therefore, we proposed the equivalent half power width using a second moment to evaluate a transmit beam using a single value.

$$W_E = 2.35E^{0.5}, \quad (2)$$

$$E = \frac{\sum [I(x) - P_T] i(x) x^2 \Delta X}{\sum [I(x) - P_T] i(x) \Delta X}, \quad (3)$$

$$i(x) = \begin{cases} 1 & \text{if } I(x) > P_T \\ 0 & \text{otherwise} \end{cases}, \quad (4)$$

where $I(x)$ is the transmit beam profile normalized to the peak intensity, and P_T is a threshold. Figure 2 shows three beam profiles with the same equivalent half power width. When a transmit beam pattern follows a Gaussian distribution, W_E is equal to the half power width of the transmit beam on the condition that $P_T = 0$. A lower value of W_E indicates a higher efficiency of the transmit power concentration at the focus. Since many aberration correction methods introduce the assumption that received signals return from a focal region, the equivalent half power width is suitable to evaluate transmit beam patterns for aberration correction.

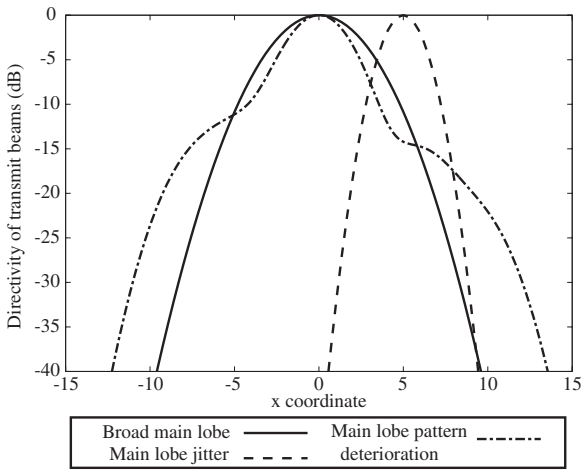

Fig. 2. Three beam profiles with the same equivalent half power width.

Sidelobes located far from the main lobe largely increase the equivalent half power width. To remove the effect of sidelobe location, we modified the equivalent half power width.

$$W_M = 2.35E_M^{0.5}, \quad (5)$$

$$E_M = \frac{\sum [I(x) - P_T] i(x) j(x)^2 \Delta X}{\sum [I(x) - P_T] i(x) \Delta X}, \quad (6)$$

$$j(x) = \begin{cases} x & \text{if } |x| < h_m/2 \\ h_m/2 & \text{otherwise} \end{cases}, \quad (7)$$

where h_m is the half power width of the main lobe under a no-aberration condition.

3. Simulation Study

3.1 Simulation model

In this study, we investigated the transmit beam patterns utilizing Spectral Flex, a computer simulation tool based on the pseudo-spectral method,[18] where the grid size of this simulation model is 0.1 mm. To evaluate the accuracy of the time delay estimation, we used ten simulated digital tissue maps, as shown in Fig. 3. The skin is 2 mm thick, the subcutaneous fat layers are 1 and 0.5 cm thick and a muscle layer exists under the subcutaneous fat layer. Fat spheres 2 mm in diameter are located randomly in the subcutaneous fat layer and account for 70% of the layer, where it is allowed to superpose a fat sphere on other spheres. Minute fat droplets of one grid in size are distributed over the muscle layer and account for 5% of the layer. A fat sphere of 1 mm in size is set at a 3 cm depth. A probe 9.5 mm wide is set at the center on the skin. The probe has 16 elements each 0.5 mm wide and the element gap is 0.1 mm. The sound velocities in muscle, fat, and connective tissue are supposed to be 1547, 1478, and 1611 m/s, respectively. We estimated the time delays for aberration correction using a transmit pulse with a -6 dB fractional bandwidth of 0.6 and center frequencies of 0.5 to 4 MHz. Figure 4 shows a transmit waveform for a 4 MHz center frequency. The focus of transmit pulses is set at the center of the fat sphere. Z_1 and Z_2, the edges of a cross-correlation window, are 2.5 and 3.5 cm, respectively.

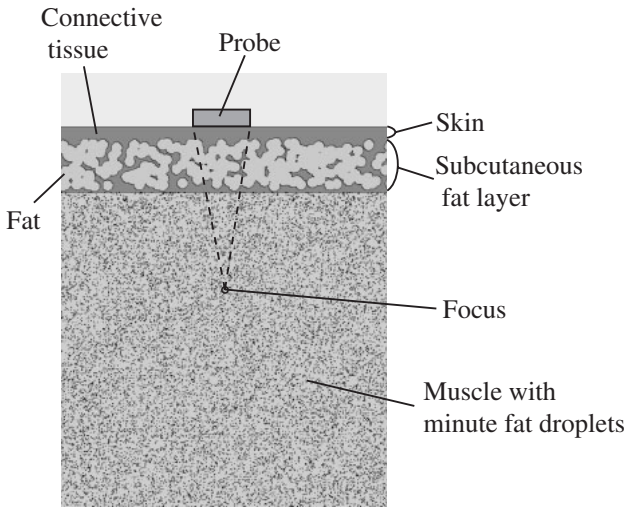

Fig. 3. Digital tissue map used in this paper. The skin consists of connective tissue. The subcutaneous fat layer 1 cm thick is composed of 30% connective tissue and 70% fat. A muscle layer with minute fat droplets exists under the fat layer. The focal range is 3 cm, and a fat sphere of 1 mm in size is placed at the focus.

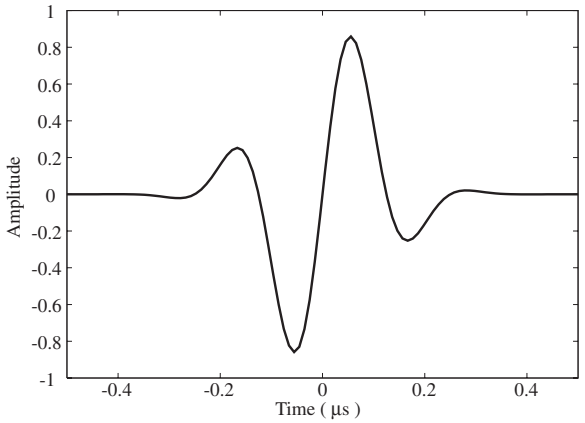

Fig. 4. Transmit waveform for a 4 MHz center frequency.

3.2 Focus quality without aberration correction

When we calculated an initial value for aberration correction, a transmit beam without aberration correction was generated. To establish a proper transmit frequency for aberration correction, we investigated the focus quality of transmit beams without aberration correction. Figure 5 shows transmit beam patterns at a focal depth of 3 cm when the subcutaneous fat layer is 1 cm thick. Figures 6 and 7 show the half power widths, main lobe jitter, and peak sidelobe levels for transmit beam patterns at different frequencies employing fat layers 1 and 0.5 cm thick, respectively. When the fat layer is 1 cm thick, the transmit beam at a 3 MHz center frequency had the narrowest beam width, and as the transmit frequency increased the sidelobe level became high. In the case employing the fat layer 0.5 cm thick, the transmit beam at a 4 MHz center frequency had the narrowest beam width, and the sidelobe level was about 7 dB lower than that employing the fat layer 1 cm thick. The equivalent half power widths of the transmit beam patterns, W_E, are shown in Figs. 8 and 9, where the thresholds set for the equivalent beam widths normalized

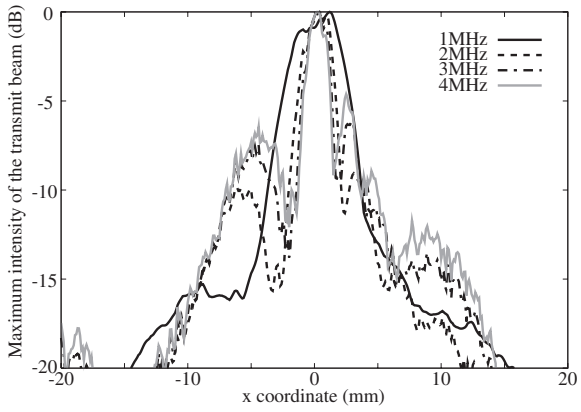

Fig. 5. Transmit beam profiles without aberration correction, where the fat layer is 1 cm thick. Transmit center frequencies are 1, 2, 3, and 4 MHz.

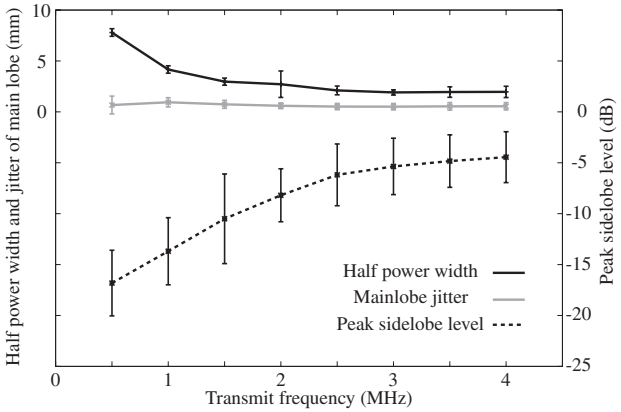

Fig. 6. Half power widths, main lobe jitter, and peak sidelobe levels for transmit beam patterns without aberration correction, where the fat layer is 1 cm thick. Data are the average of 10 simulations using different digital tissue maps, and the error bar shows the standard deviation.

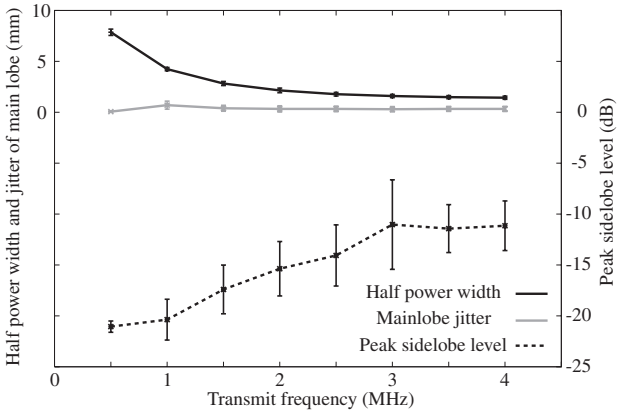

Fig. 7. Half power widths, main lobe jitter, and peak sidelobe levels for transmit beam patterns without aberration correction, where the fat layer is 0.5 cm thick. Data are the average of 10 simulations using different digital tissue maps, and the error bar shows the standard deviation.

to the peak main lobe power were −20, −15, and −10 dB. When the fat layer is 1 cm thick the high sidelobe level at high transmit frequencies accounts for the transmit beam at a 1.5 MHz center frequency having the lowest value of W_E,

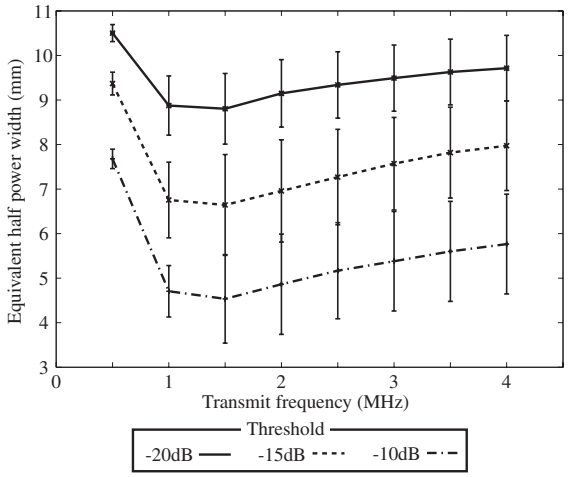

Fig. 8. Equivalent half power widths for transmit beam patterns without aberration correction, where the fat layer is 1 cm thick. Data are the average of 10 simulations using different digital tissue maps. The error bar shows half of the standard deviation.

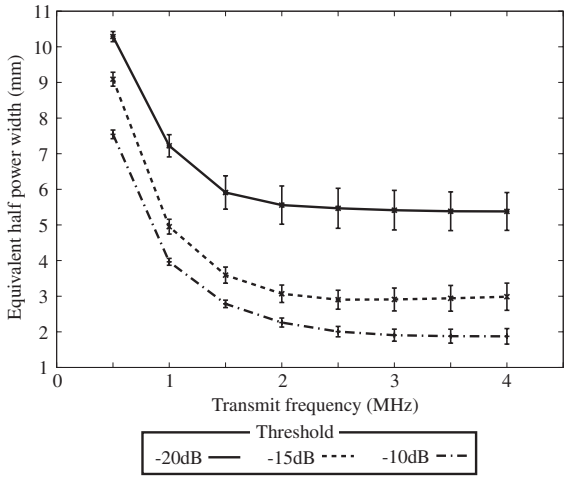

Fig. 9. Equivalent half power widths for transmit beam patterns without aberration correction, where a fat layer is 0.5 cm thick. Data are the average of 10 simulations using different digital tissue maps. Error bar shows the half of the standard deviation.

i.e., the highest efficiency of the transmit power concentration at the focus. This implied that the proper transmit frequency in this condition was about 1.5 MHz. On the other hand, in the case employing the fat layer 0.5 cm thick the transmit beam at a 4 MHz center frequency had the lowest value of W_E, and the transmit beams with the center frequency of more than 2 MHz had adequately low values of W_E. Consequently, W_E increased significantly when the transmit frequency was more than 2 MHz.

3.3 Focus quality with aberration correction using low-frequency transmission

A transmit beam with a low center frequency is considered to be less affected by aberration. Therefore, we employed a focused transmit beam of a low center frequency for aberration correction. The aberration correction value set was applied to the following imaging process utilizing a high transmit frequency. Figure 10 shows transmit beam profiles

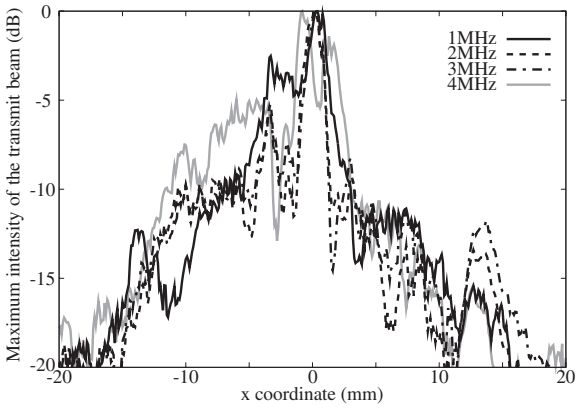

Fig. 10. Transmit beam profiles with aberration correction in the case employing a fat layer 1 cm thick, where the transmit center frequency is 4 MHz. In the aberration correction process, transmit frequencies of 1 and 4 MHz were employed.

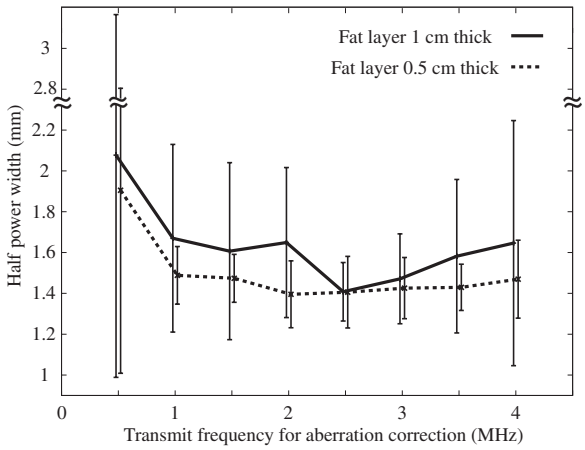

Fig. 11. Half power widths of the transmit beams at a 4 MHz center frequency with aberration correction, where fat layers are 1 and 0.5 cm thick. In the aberration correction process, transmit frequencies of 0.5 to 4 MHz are employed. Data are the average of 10 simulations, and the error bar shows the standard deviation.

with aberration correction at a focal depth of 3 cm in the case employing a fat layer 1 cm thick, where the center frequency of transmit pulses was 4 MHz. Figure 11 shows the half power widths of the transmit beams at a 4 MHz center frequency with aberration correction. In the aberration correction processes, transmit pulses with center frequencies of 0.5 to 4 MHz were generated without aberration correction. Since the transmit frequency is constant in the second transmission, the main lobe width of the transmit beam profile is fixed. We thus utilized the modified equivalent half power width for the investigation of the transmit beam pattern in the second transmission. Since the main lobe width of the transmit beam profile at the 4 MHz center frequency is 3 mm in a no-aberration condition, we set h_m as 3 mm. Figures 12 and 13 show the modified equivalent beam width of the transmit beams with aberration correction employing fat layers of 1 and 0.5 cm, respectively. These results indicate that the optimum transmit center frequency for aberration correction was about 2 MHz in the simulation model used in this study, much lower than the transmit frequency for imaging.

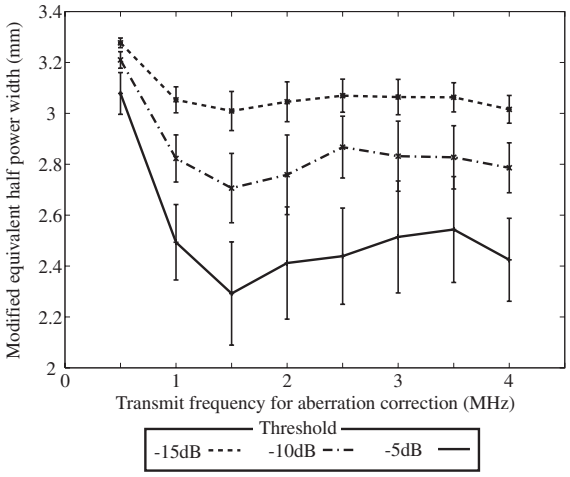

Fig. 12. Modified equivalent half power width of transmit beam patterns with aberration correction, where the fat layer is 1 cm thick and the transmit center frequency is 4 MHz. Data are the average of 10 simulations using different digital tissue maps. The error bar shows quarter of the standard deviation. In the aberration correction process, transmit frequencies of 0.5 to 4 MHz are employed.

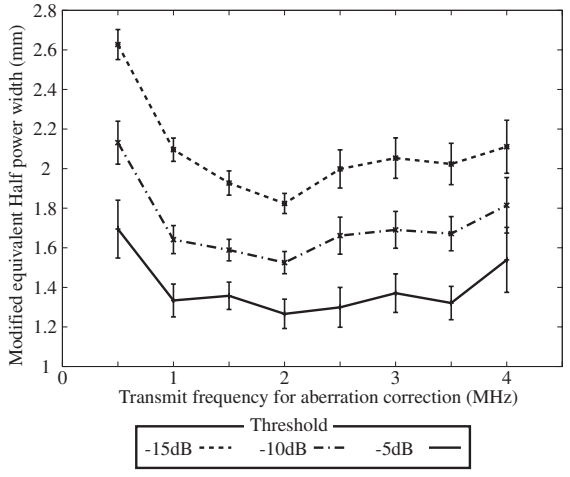

Fig. 13. Modified equivalent half power width of transmit beam patterns with aberration correction, where the fat layer is 0.5 cm thick and the transmit center frequency is 4 MHz. Data are the average of 10 simulations using different digital tissue maps. The error bar shows quarter of the standard deviation. In the aberration correction process, transmit frequencies of 0.5 to 4 MHz are employed.

4. Discussion

In this paper, we proposed an aberration correction technique using a lower transmit frequency than that for imaging. To evaluate the improvement of focus quality under aberration conditions, we introduced the equivalent half power width, an evaluation criterion using the second moment of beam profiles. First, we surveyed the focus quality for various transmit frequencies under aberration conditions. It is difficult to grade the focus quality of beam patterns with aberration from the conventional evaluation factors of main lobe width, main lobe jitter, and peak sidelobe level. In contrast, the equivalent half power width presents an evaluation of beam patterns with aberration. From this evaluation we confirmed that a beam pattern of lower transmit frequency is less affected by aberration.

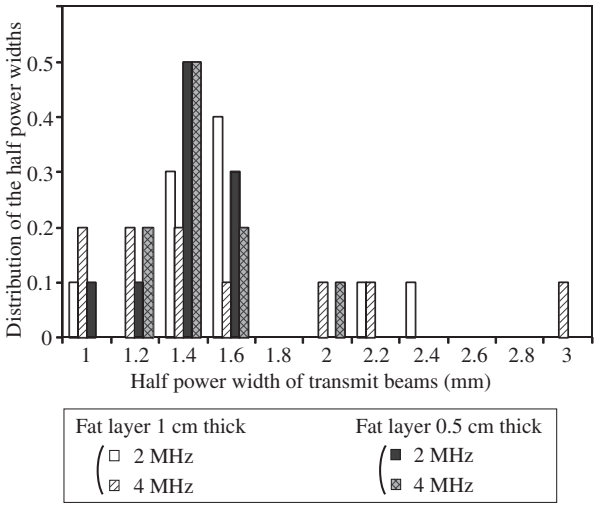

Fig. 14. Distribution of half power widths of transmit beam patterns at a 4 MHz center frequency with aberration correction, where the transmit frequencies for aberration correction are 2 and 4 MHz.

We calculated eight aberration correction values using cross-correlation between two received signals of adjacent elements from eight different frequency transmissions of 0.5 to 4 MHz, and employed them for beam forming with a 4 MHz frequency transmission. The results show that the transmit frequencies of 1.5 and 2 MHz are suitable for the aberration correction in imaging using a 4 MHz transmit frequency, where the cutaneous fat layers are respectively 1 and 0.5 cm thick and the focal range is 3 cm. Figure 14 shows the distribution of half power widths of transmit beam patterns at a 4 MHz center frequency with aberration correction, where the transmit frequencies for aberration correction are 2 and 4 MHz. When the transmit frequency for aberration correction is 4 MHz the transmit beam pattern with aberration correction sometimes deteriorates markedly. This deterioration of transmit beam pattern is caused by a failure of estimation of arrival time difference between two adjacent elements originated from the decorrelation between received signals at the two adjacent elements. The initial value set for aberration correction should be close to the true value set. Therefore, these results imply the validity of low-frequency transmission for aberration correction, particularly to calculate an initial value set for aberration correction under a severe aberration condition.

5. Conclusions

In this study, we proposed an aberration correction technique using lower frequency transmission than that for imaging, and introduced a criterion to evaluate the focus quality of beam patterns under aberration conditions. Simulation studies show that the transmit center frequencies of 1.5 and 2 MHz are suitable for aberration correction in the cases of fat layers 1 and 0.5 cm thick. This study implies that under severe aberration conditions, the proper transmit frequency for the aberration condition is lower than half of that for imaging.

Acknowledgments

This work was supported in part by a Grant-in-Aid for Scientific Research from the Ministry of Education, Culture,

Sport, Science and Technology, and by the Innovative Techno-Hub for Integrated Medical Bio-imaging Project of the Special Coordination Funds for Promoting Science and Technology, from the Ministry of Education, Culture, Sports, Science and Technology, Japan (MEXT).

1) Y. Abe, H. Hasegawa, and H. Kanai: Jpn. J. Appl. Phys. **46** (2007) 4813.
2) K. Nogami and A. Yamada: Jpn. J. Appl. Phys. **46** (2007) 4820.
3) H. Taki and T. Sato: Jpn. J. Appl. Phys. **46** (2007) 4827.
4) T. Kimura, H. Taki, T. Sakamoto, and T. Sato: Jpn. J. Appl. Phys. **48** (2009) 07GJ07.
5) T. Christopher: IEEE Trans. Ultrason. Ferroelectr. Freq. Control **44** (1997) 125.
6) C.-C. Shen and P.-C. Li: IEEE Trans. Ultrason. Ferroelectr. Freq. Control **48** (2001) 728.
7) S. J. Rosenthal, P. H. Jones, and L. H. Wetzel: Am. J. Roentgenol. **176** (2001) 1393.
8) T. Hosono, Y. Chiba, H. Kanai, and T. Kanagawa: Ultrasound Obstet. Gynecol. **19** (2002) 400.
9) T. Varslot, S.-E. Måsøy, and B. Angelsen: Proc. IEEE Ultrasonics Symp., 2005, Vol. 2, p. 1327.
10) T. Varslot, S.-E. Måsøy, T. F. Johansen, and B. Angelsen: IEEE Trans. Ultrason. Ferroelectr. Freq. Control **54** (2007) 470.
11) S. W. Flax and M. O'Donnell: IEEE Trans. Ultrason. Ferroelectr. Freq. Control **35** (1988) 758.
12) M. O'Donnell and S. W. Flax: IEEE Trans. Ultrason. Ferroelectr. Freq. Control **35** (1988) 768.
13) S. E. Måsøy, T. Varslot, and B. Angelsen: J. Acoust. Soc. Am. **117** (2005) 450.
14) S. E. Måsøy, T. Varslot, and B. Angelsen: J. Acoust. Soc. Am. **115** (2004) 2998.
15) T. Varslot, E. Mo, H. Krogstad, and B. Angelsen: J. Acoust. Soc. Am. **115** (2004) 3068.
16) S. Krishnan, K. W. Rigby, and M. O'Donnell: IEEE Trans. Ultrason. Ferroelectr. Freq. Control **45** (1998) 691.
17) R. Mallart and M. Fink: J. Acoust. Soc. Am. **96** (1994) 3721.
18) Q. H. Liu: IEEE Trans. Ultrason. Ferroelectr. Freq. Control **45** (1998) 1044.